PHYSICAL REVIEW D **89,** 124034 (2014)

Dynamics of the post-Newtonian circular restricted three-body problem with compact objects

Guoqing Huang and Xin Wu*

Department of Physics, School of Civil Engineering and Architecture, Institute of Astronomy, Nanchang University, Nanchang 330031, China

(Received 2 January 2014; published 27 June 2014)

By applying scaling transformations to distance and time, we obtain the first post-Newtonian equations of motion for a relativistic circular restricted three-body problem, where the Newtonian terms do not depend on the separation of a parent binary, though the post-Newtonian terms do. The post-Newtonian contributions consist of the relativistic effects from the circular orbital frequencies between the primaries and those from the primaries to a third body. When the former post-Newtonian contribution and the nonrelativistic terms are considered, the post-Newtonian dynamics are qualitatively different from the Newtonian dynamics if the separation between the two primaries is insufficiently large. When the latter post-Newtonian contribution is also included, some orbits become unstable. By scanning the dependence of the dynamics on the separation with fast Lyapunov indicators, the separation is classified into three domains for dynamically unstable, bounded chaotic, and bounded regular dynamics.

DOI: 10.1103/PhysRevD.89.124034 PACS numbers: 04.25.Nx, 05.45.-a, 95.10.Fh, 97.60.Lf

I. INTRODUCTION

In the early 20th century, Einstein's general relativity successfully accounted for the previously unexplained discrepancy between observations of the advance of the perihelion of Mercury's orbit and the predictions of Newtonian mechanics. Since then, it has been regarded as a more accurate theory of gravity than that of Newton. As mentioned in Refs. [1–4], the influence exerted by general relativity upon the dynamics of the bodies in our Solar System should not be neglected. In particular, Wanex [2] demonstrated that the difference between the final positions of Newtonian and relativistic trajectories in the restricted three-body problem made of a space probe, the Earth, and the Moon becomes considerably larger for bounded chaotic orbits than for bounded regular orbits. This is the so-called "chaotic amplification effect" in the relativistic problem. Note that post-Newtonian (PN) approximations of general relativistic systems were mainly used because Einstein's field equations cannot be rigorously solved in most cases.

The onset of strong chaos in compact objects, including neutron stars and black holes, can be found in many references (see, e.g., Refs. [5–8]). The chaotic dynamics of PN conservative systems of binary spinning compact objects are clearly understood [9–12]. Moreover, there are several authors [9,10,13,14] who have tried to use extreme sensitivity to initial spin angles in fractal basin boundaries to signal the onset of chaos during the final orbits before the merger of the binary when 2.5PN radiation reaction effects are included. However, whether the chaotic behavior found in the nondissipative 2PN dynamics can leave an imprint on the dissipative 2.5PN dynamics remains unclear since the fractal basin boundary method itself is built on an unstable, fractal set of orbits. Other methods, such as surface of section and Lyapunov exponents, are not useful for a dissipative system. The method of surface of section is effective for a conservative system whose phase space has four dimensions, but a two-dimensional surface of section cannot be obtained because of energy loss that leads to a shrinking orbital radius, and Lyapunov exponents cannot distinguish instability caused by the onset of chaos from instability because of merger caused by energy emission. As claimed in Ref. [10], "There is no clear way to identify irregular behavior in merging binaries when dissipation is included."

Recently, the PN effects on Lagrange's collinear solutions and the equilateral triangular solution of the three-body problem were investigated [15,16]. The compact three-body dynamics with gravitational-wave emission was also considered. For example, Wardell [17,18] studied resonance behaviors between the binary and third-mass orbits when the effects of gravitational radiation reaction were included in a classical three-body system. Schnittman [19] discussed the location and stability of the Lagrange equilibrium points, L_4 and L_5, in the circular restricted three-body problem with gravitational radiation losses from two massive bodies. There were similar conclusions when the 1PN terms were further added [20]. However, chaos in the PN three-body problems was never discussed in these studies.

It is worth emphasizing that the separation of the primaries and angular speeds of the primaries with respect to an inertial frame in the PN equations of motion for the

*xwu@ncu.edu.cn

circular restricted three-body problem were directly considered as one geometric unit in Ref. [1]. Therefore, the PN contributions seem to be independent of the separation and angular speed. In this study, we let the PN contributions appear in the PN system and apply scaling transformations to distance and time so that the Newtonian terms do not depend on the separation, but the post-Newtonian terms do. Since it is difficult to identify chaotic behavior in merging orbits with radiative reaction, we shall look for chaotic behavior when the system is conservative and the radiation reaction is turned off. Thus, we shall investigate how the separation affects the dynamics of order and chaos in the PN circular restricted three-body problem.

II. POST-NEWTONIAN EQUATIONS

On the basis of the PN gravitational theory of Einstein, Infeld, and Hoffmann [21], the Lagrangian L_{k+1} for a single body m, with position $\mathbf{r}$ and velocity $\mathbf{u}$, in a gravitational field produced by k other bodies is

$$\begin{aligned} L_{k+1} = & -mc^2 + \frac{1}{2}m\mathbf{u}^2 + Gm\sum_{i=1}^{k}\frac{m_i}{|\mathbf{r}-\mathbf{r}_i|} \\ & + \frac{1}{8c^2}m\mathbf{u}^4 - \frac{G^2m}{2c^2}\left(\sum_{i=1}^{k}\frac{m_i}{|\mathbf{r}-\mathbf{r}_i|}\right)^2 \\ & - \frac{Gm}{2c^2}\sum_{i=1}^{k}\frac{m_i}{|\mathbf{r}-\mathbf{r}_i|}\cdot\Big[7(\mathbf{u}\cdot\mathbf{u}_i) \\ & + (\mathbf{n}_i\cdot\mathbf{u})(\mathbf{n}_i\cdot\mathbf{u}_i) - 3(\mathbf{u}^2+\mathbf{u}_i^2) \\ & + 2G\sum_{j\neq i}^{k}\frac{m_j}{|\mathbf{r}_i-\mathbf{r}_j|}\Big] + O(c^{-4}), \end{aligned} \tag{1}$$

where m and m_i are the masses of these bodies, c denotes the velocity of light, G stands for the gravitational constant, and the unit vector from body i to body $k+1$ is $\mathbf{n}_i = (\mathbf{r}-\mathbf{r}_i)/|\mathbf{r}-\mathbf{r}_i|$.

Let us consider a planar circular restricted three-body problem in which two primaries, having a separation a, move in circular orbits around their center of mass with an angular speed ω relative to an inertial frame, and a third mass, m, is so small that it does not perturb the circular motions of the binary; in other words, the two primaries affect the third body gravitationally, but the third body does not have any gravitational effect upon the two primaries [22]. We take $m_1+m_2=M$, dimensionless masses $\mu_1 = m_1/M$ and $\mu_2 = m_2/M$, and the geometrized unit $G=1$. Note that we continue to use c so as to clearly show the PN contributions in this section, and take $c=1$ in our later numerical simulations. To adopt dimensionless variables, we assume that the distance and time t are measured in terms of M. Because of the circular motions, bodies 1 and 2 have position coordinates $\mathbf{r}_1 = (\bar{X}_1\cos\omega t, \bar{X}_1\sin\omega t)$ and $\mathbf{r}_2 = (\bar{X}_2\cos\omega t, \bar{X}_2\sin\omega t)$, with $\bar{X}_1 = -a\mu_2$ and $\bar{X}_2 = a\mu_1$, and velocities $\mathbf{u}_1 = (-\bar{X}_1\omega\sin\omega t, \bar{X}_1\omega\cos\omega t)$ and $\mathbf{u}_2 = (-\bar{X}_2\omega\sin\omega t, \bar{X}_2\omega\cos\omega t)$ in the inertial frame. In the rotating frame, their positions and velocities become $\bar{\mathbf{R}}_1 = (\bar{X}_1, 0)$, $\bar{\mathbf{R}}_2 = (\bar{X}_2, 0)$, $\bar{\mathbf{U}}_1 = (0, \bar{X}_1\omega)$, and $\bar{\mathbf{U}}_2 = (0, \bar{X}_2\omega)$. For the third body as a test particle, the position $\mathbf{r} = (x, y)$ and velocity $\mathbf{u} = (\dot{x}, \dot{y})$ in the inertial frame can be transformed into the position $\bar{\mathbf{R}} = (\bar{X}, \bar{Y})$ and the velocity $\bar{\mathbf{U}} = (\dot{\bar{X}}, \dot{\bar{Y}})$ in the rotating frame,

$$\begin{aligned} x &= \bar{X}\cos\omega t - \bar{Y}\sin\omega t, \\ y &= \bar{X}\sin\omega t + \bar{Y}\cos\omega t, \\ \dot{x} &= (\dot{\bar{X}} - \omega\bar{Y})\cos\omega t - (\dot{\bar{Y}} + \omega\bar{X})\sin\omega t, \\ \dot{y} &= (\dot{\bar{X}} - \omega\bar{Y})\sin\omega t + (\dot{\bar{Y}} + \omega\bar{X})\cos\omega t. \end{aligned} \tag{2}$$

The Lagrangian of the third body in the rotating frame is $\bar{L} = (L_3 + mc^2)/m$, i.e.,

$$\begin{aligned} \bar{L} &= \frac{\mu_1}{d_1} + \frac{\mu_2}{d_2} + \frac{1}{2}(\bar{U}^2 + 2\bar{A}\omega + \bar{R}^2\omega^2) + \frac{1}{c^2}\bar{L}_2, \\ d_1 &= \sqrt{(\bar{X}-\bar{X}_1)^2 + \bar{Y}^2}, \\ d_2 &= \sqrt{(\bar{X}-\bar{X}_2)^2 + \bar{Y}^2}, \\ \bar{U}^2 &= \dot{\bar{X}}^2 + \dot{\bar{Y}}^2, \\ \bar{A} &= \dot{\bar{Y}}\bar{X} - \dot{\bar{X}}\bar{Y}, \\ \bar{R}^2 &= \bar{X}^2 + \bar{Y}^2. \end{aligned} \tag{3}$$

The PN part $\bar{L}_2$ has a long expression given by the following equation:

$$\begin{aligned} \bar{L}_2 = & \frac{1}{8}(\bar{U}^2 + 2\bar{A}\omega + \bar{R}^2\omega^2)^2 - \frac{\mu_1\mu_2}{a}\left(\frac{1}{d_1} + \frac{1}{d_2}\right) \\ & - \left(\frac{\mu_1^2}{2d_1^2} + \frac{\mu_2^2}{2d_2^2} + \frac{\mu_1\mu_2}{d_1d_2}\right) + \frac{3}{2}\left(\frac{\mu_1}{d_1} + \frac{\mu_2}{d_2}\right) \\ & \cdot(\bar{U}^2 + 2\bar{A}\omega + \bar{R}^2\omega^2) + \frac{3}{2}\omega^2\left(\frac{\mu_1\bar{X}_1^2}{d_1} + \frac{\mu_2\bar{X}_2^2}{d_2}\right) \\ & - \frac{7}{2}\omega(\dot{\bar{Y}} + \omega\bar{X})\left(\frac{\mu_1\bar{X}_1}{d_1} + \frac{\mu_2\bar{X}_2}{d_2}\right) - \frac{1}{2}\omega\bar{Y}(\dot{\bar{X}} - \omega\bar{Y}) \\ & \cdot\left[\frac{\mu_1\bar{X}_1(\bar{X}-\bar{X}_1)}{d_1^3} + \frac{\mu_2\bar{X}_2(\bar{X}-\bar{X}_2)}{d_2^3}\right] \\ & - \frac{1}{2}\omega\bar{Y}^2(\dot{\bar{Y}} + \omega\bar{X})\left(\frac{\mu_1\bar{X}_1}{d_1^3} + \frac{\mu_2\bar{X}_2}{d_2^3}\right). \end{aligned} \tag{4}$$

The angular speed ω of the primaries in the first line of Eq. (3) (which was given in Ref. [1]) is

$$\omega = \omega_0(1 + \omega_1/c^2), \tag{5}$$

$$\omega_0 = a^{-3/2}, \tag{6}$$

$$\omega_1 = (\mu_1\mu_2 - 3)/(2a), \tag{7}$$

$$\omega^2 = \omega_0^2(1 + 2\omega_1/c^2). \tag{8}$$

Here, ω_0 and $\omega_0\omega_1$ are the Newtonian angular speeds of the primaries and the PN angular velocity, respectively. However, $\omega = \omega_0$ in Eq. (4) because $\bar{L}_2$ is accurate to the 1PN level. Substituting Eqs. (5) and (8) into the first line of Eq. (3), we split the Lagrangian into three parts,

$$\bar{L} = \bar{L}_0 + c^{-2}\bar{L}_1 + c^{-2}\bar{L}_2, \tag{9}$$

$$\bar{L}_0 = \frac{\mu_1}{d_1} + \frac{\mu_2}{d_2} + \frac{1}{2}(\bar{U}^2 + 2\bar{A}\omega_0 + \bar{R}^2\omega_0^2), \tag{10}$$

$$\bar{L}_1 = \omega_0\omega_1(\bar{A} + \bar{R}^2\omega_0). \tag{11}$$

Obviously, $\bar{L}_0$ represents the Newtonian restricted three-body problem [22]. $\bar{L}_1$ is a PN contribution to the circular orbital frequency between the primaries, and $\bar{L}_2$, with $\omega = \omega_0$, is another PN contribution from the primaries to the third body. In other words, the 1PN terms between bodies 1 and 2, those from body 1 to body 3, and those from body 2 to body 3 are all considered, whereas the 1PN terms from body 3 to bodies 1 and 2 are neglected. This consideration for incorporating these fully 1PN-accurate equations is based on the case of the two primaries having comparable masses. If $m_1 \gg m_2$, we are interested only in the cross PN terms between the central body 1 and body 2 and those between the central body 1 and body 3, and not in the PN terms between bodies 2 and 3, because the former PN contributions are more important than the latter ones. The PN terms between bodies 2 and 3 have no effect on the results and are computationally troublesome. Therefore, they can be neglected; that is, neither $\bar{L}_2$ with $\omega = \omega_0$ in Eq. (4) nor ω_1 in Eq. (7) contains any term associated with the factor μ_2. This suggestion was borrowed from a recent paper by Will [23].

The Lagrangian equations of motion derived from Eq. (9), as the PN equations of motion for body 3, are given by the following equation:

$$\frac{d}{dt}\frac{\partial \bar{L}}{\partial \dot{\bar{X}}} = \frac{\partial \bar{L}}{\partial \bar{X}}, \qquad \frac{d}{dt}\frac{\partial \bar{L}}{\partial \dot{\bar{Y}}} = \frac{\partial \bar{L}}{\partial \bar{Y}}. \tag{12}$$

Their detailed expressions are

$$\ddot{\bar{X}} = \left[\omega_0(2\dot{\bar{Y}} + \omega_0\bar{X}) - \frac{\mu_1(\bar{X} - \bar{X}_1)}{d_1^3} - \frac{\mu_2(\bar{X} - \bar{X}_2)}{d_2^3}\right] + 2\omega_0\omega_1(\dot{\bar{Y}} + \omega_0\bar{X})c^{-2} + \bar{P}c^{-2}, \tag{13}$$

$$\ddot{\bar{Y}} = \left[\omega_0(\omega_0\bar{Y} - 2\dot{\bar{X}}) - \bar{Y}\left(\frac{\mu_1}{d_1^3} + \frac{\mu_2}{d_2^3}\right)\right] + 2\omega_0\omega_1(\omega_0\bar{Y} - \dot{\bar{X}})c^{-2} + \bar{Q}c^{-2}, \tag{14}$$

where $\bar{P}$ and $\bar{Q}$ are derived from $\bar{L}_2$ and are given by the following equations:

$$\begin{aligned}\bar{P} = {} & 6\omega_0\left(\frac{\mu_1}{d_1} + \frac{\mu_2}{d_2}\right)\left(\dot{\bar{Y}} + \frac{1}{2}\omega_0\bar{X}\right) + \frac{\mu_1\mu_2}{a}\cdot\left(\frac{\bar{X} - \bar{X}_1}{d_1^3} + \frac{\bar{X} - \bar{X}_2}{d_2^3}\right) + \omega_0\left(4\dot{\bar{Y}} + \frac{7}{2}\omega_0\bar{X}\right)\cdot\left[\frac{\mu_1\bar{X}_1(\bar{X} - \bar{X}_1)}{d_1^3} + \frac{\mu_2\bar{X}_2(\bar{X} - \bar{X}_2)}{d_2^3}\right] \\ & + \left[\frac{\mu_1(\bar{X} - \bar{X}_1)}{d_1^3} + \frac{\mu_2(\bar{X} - \bar{X}_2)}{d_2^3}\right]\left[\frac{\mu_1}{d_1} + \frac{\mu_2}{d_2} - \frac{3}{2}(\bar{U}^2 + 2\bar{A}\omega_0 + \bar{R}^2\omega_0^2) + 3\dot{\bar{X}}(\dot{\bar{X}} - \omega_0\bar{Y})\right] - 3\omega_0(2\dot{\bar{Y}} + \omega_0\bar{X})\left(\frac{\mu_1}{d_1} + \frac{\mu_2}{d_2}\right) \\ & + \left[\frac{\mu_1(\bar{X} - \bar{X}_1)}{d_1^3} + \frac{\mu_2(\bar{X} - \bar{X}_2)}{d_2^3}\right]\left[3\left(\frac{\mu_1}{d_1} + \frac{\mu_2}{d_2}\right) + \frac{1}{2}(\bar{U}^2 + 2\bar{A}\omega_0 + \bar{R}^2\omega_0^2) + (\dot{\bar{X}} - \omega_0\bar{Y})^2\right] \\ & + 3\left(\frac{\mu_1}{d_1^3} + \frac{\mu_2}{d_2^3}\right)\dot{\bar{Y}}\cdot(\dot{\bar{X}} - \omega_0\bar{Y})\bar{Y} - \frac{7}{2}\omega_0^2\left(\frac{\mu_1\bar{X}_1}{d_1} + \frac{\mu_2\bar{X}_2}{d_2}\right) - \frac{3}{2}\omega_0^2\left[\frac{\mu_1\bar{X}_1^2(\bar{X} - \bar{X}_1)}{d_1^3} + \frac{\mu_2\bar{X}_2^2(\bar{X} - \bar{X}_2)}{d_2^3}\right] \\ & + \frac{3}{2}\omega_0^2\bar{Y}^2\left[\frac{\mu_1\bar{X}_1^2(\bar{X} - \bar{X}_1)}{d_1^5} + \frac{\mu_2\bar{X}_2^2(\bar{X} - \bar{X}_2)}{d_2^5}\right] - \left(\frac{\mu_1}{d_1^3} + \frac{\mu_2}{d_2^3}\right)(\dot{\bar{Y}} + \omega_0\bar{X})(\omega_0\bar{Y} - \dot{\bar{X}})\bar{Y},\end{aligned} \tag{15}$$

$$\begin{aligned}\bar{Q} = {} & -\left(\frac{\mu_1\bar{X}_1}{d_1^3} + \frac{\mu_2\bar{X}_2}{d_2^3}\right)\left[3\dot{\bar{X}}\dot{\bar{Y}} + 7\omega_0\bar{X}\left(\dot{\bar{X}} - \frac{1}{2}\omega_0\bar{Y}\right)\right] + \omega_0\left(\frac{\mu_1\bar{X}_1^2}{d_1^3} + \frac{\mu_2\bar{X}_2^2}{d_2^3}\right)\left(4\dot{\bar{X}} - \frac{5}{2}\omega_0\bar{Y}\right) + \frac{\mu_1\mu_2}{a}\bar{Y}\left(\frac{1}{d_1^3} + \frac{1}{d_2^3}\right) + \frac{3}{2}\omega_0^2\bar{Y}^3 \\ & \cdot\left(\frac{\mu_1\bar{X}_1^2}{d_1^5} + \frac{\mu_2\bar{X}_2^2}{d_2^5}\right) - (\dot{\bar{Y}} + \omega_0\bar{X})(\omega_0\bar{Y} - \dot{\bar{X}})\left[\frac{\mu_1(\bar{X} - \bar{X}_1)}{d_1^3} + \frac{\mu_2(\bar{X} - \bar{X}_2)}{d_2^3}\right] + \left(\frac{\mu_1}{d_1^3} + \frac{\mu_2}{d_2^3}\right)\left\{\bar{Y}\left[4\left(\frac{\mu_1}{d_1} + \frac{\mu_2}{d_2}\right)\right.\right. \\ & \left.\left. - (\bar{U}^2 + 2\bar{A}\omega_0 + \bar{R}^2\omega_0^2) + (\dot{\bar{Y}} + \omega_0\bar{X})^2\right] + 3(\dot{\bar{Y}} + \omega_0\bar{X})\cdot(\dot{\bar{X}}\bar{X} + \dot{\bar{Y}}\bar{Y})\right\}.\end{aligned} \tag{16}$$

It should be pointed out that $\bar{P}$ and $\bar{Q}$ are functions of a and ω_0, labeled as $\bar{P}(a,\omega_0)$ and $\bar{Q}(a,\omega_0)$. In addition, the PN equations of motion given by Eqs. (13)–(16) are slightly different from those given in Ref. [1], where a and ω_0 were either set to 1 or were missing entirely.

To guarantee that both the distance of the binary and the angular velocity of the binary with respect to the inertial frame in the Newtonian restricted three-body problem are set to one geometric unit, we transform the distance and time as $\bar{X} = aX$, $\bar{Y} = aY$, and $t = \tau/\omega_0$. In other words, the units of the new space and time variables are a and $1/\omega_0$, respectively. In this case, we have $\dot{\bar{X}} = a\omega_0 X'$, $\dot{\bar{Y}} = a\omega_0 Y'$, $\ddot{\bar{X}} = a\omega_0^2 X''$, and $\ddot{\bar{Y}} = a\omega_0^2 Y''$, where a prime denotes a derivative with respect to the new time variable τ. On the basis of Eqs. (15) and (16), we obtain $P = \bar{P}(1,1)$ and $Q = \bar{Q}(1,1)$ by dropping all bars over the letters like A and replacing $\dot{\bar{X}}$ and $\dot{\bar{Y}}$ with X' and Y'. Using these scaling transformations to distance, time, velocity, and acceleration, we can readjust Eqs. (13) and (14) as follows:

$$X'' = \left[2Y' + X - \frac{\mu_1(X-X_1)}{D_1^3} - \frac{\mu_2(X-X_2)}{D_2^3}\right] + 2\omega_1(Y'+X)c^{-2} + (P/a)c^{-2}, \tag{17}$$

$$Y'' = \left[Y - 2X' - Y\left(\frac{\mu_1}{D_1^3} + \frac{\mu_2}{D_2^3}\right)\right] + 2\omega_1(Y-X')c^{-2} + (Q/a)c^{-2}, \tag{18}$$

where $X_1 = -\mu_2$, $X_2 = \mu_1$, and

$$D_1 = \sqrt{(X-X_1)^2 + Y^2},$$
$$D_2 = \sqrt{(X-X_2)^2 + Y^2}. \tag{19}$$

Here are three points of illustration. (i) The terms in the square brackets, the ω_1 terms, and the P and Q terms in Eqs. (17) and (18) are derived from the Newtonian Lagrangian L_0, the PN Lagrangian L_1 caused by the relativistic effects between the primaries, and the PN Lagrangian L_2 from the relativistic effects on the primaries to the third body, respectively. Thus, there is the total Lagrangian $L = L_0 + L_1 + L_2$. (ii) Maindl and Dvorak [1] directly used the customary units of $a = \omega_0 = 1$; however, we adopt scaling transformations that can completely satisfy this requirement. In particular, an explicit difference between the two treatments lies in the fact that our PN Lagrangians, L_1 and L_2, depend on the separation a, unlike theirs. This lets us investigate how the separation affects the dynamics of the PN restricted three-body problem L. (iii) L_0 corresponds to the Jacobian constant [22]

$$C_J = X^2 + Y^2 + 2\left(\frac{\mu_1}{D_1} + \frac{\mu_2}{D_2}\right) - X'^2 - Y'^2; \tag{20}$$

similarly, L also holds its PN Jacobian constant, which can be found in Ref. [1]. However, the PN Jacobian constant is not exactly conserved, but it is approximately conserved in the 1PN level.

III. THE PN LAGRANGIAN DYNAMICS

An eighth- and ninth-order Runge-Kutta-Fehlberg algorithm [RKF8(9)] with a variable time step is used to integrate Eqs. (17) and (18). First, we consider its application to the Newtonian problem, L_0, and take the Newtonian Jacobian constant $C_J = 3.07$, the mass parameter $\mu_2 = 10^{-3}$, orbit 1 with initial values $X = 0.55$, $Y = 0$, $X' = 0$, and $Y' > 0$ given by Eq. (20), and orbit 2 with only slightly different initial values of $X = 0.56$, and Y and X' unchanged. RKF8(9) performs well because it can give a value for the Jacobian constant that is accurate to a magnitude of order 10^{-12} or so for both orbit 1 and orbit 2 when the integration time τ reaches 10^6. In fact, orbit 1, made of three islands, is ordered, but orbit 2 is chaotic, as shown by the Poincaré surface of section in Fig. 1. The features of the two orbits can also be found in Ref. [22]. It is not easy to find the onset of chaos for $a > 1$ if the nonscaling Newtonian problem, $\bar{L}_0$, which depends on the separation and angular speed of the primaries, is solved numerically. This is why we used the scaled equations (17) and (18). Besides the two orbits, chaotic orbit 3 with two unstable hyperbolic fixed points and a regular orbit 4 with a quasiperiodic Kolmogorov-Arnold-Moser (KAM) torus are

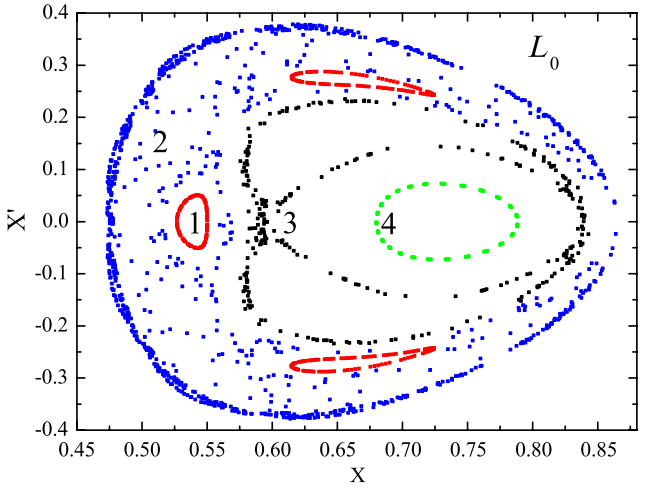

FIG. 1 (color online). Poincaré surface of section on the plane $Y = 0$ with $Y' > 0$ for four trajectories in the Newtonian circular restricted three-body problem, L_0, with the Jacobian constant $C_J = 3.07$ and the mass $\mu_2 = 0.001$. Orbits 1, 2, 3, and 4 have initial values $Y = 0$ and $X' = 0$ and their starting values of X are 0.55, 0.56, 0.60, and 0.68, respectively. Orbit 1 (consisting of three islands) and orbit 4 (with a torus) are typically regular, but orbits 2 and 3—with many points covering a larger region—turn out to be chaotic.

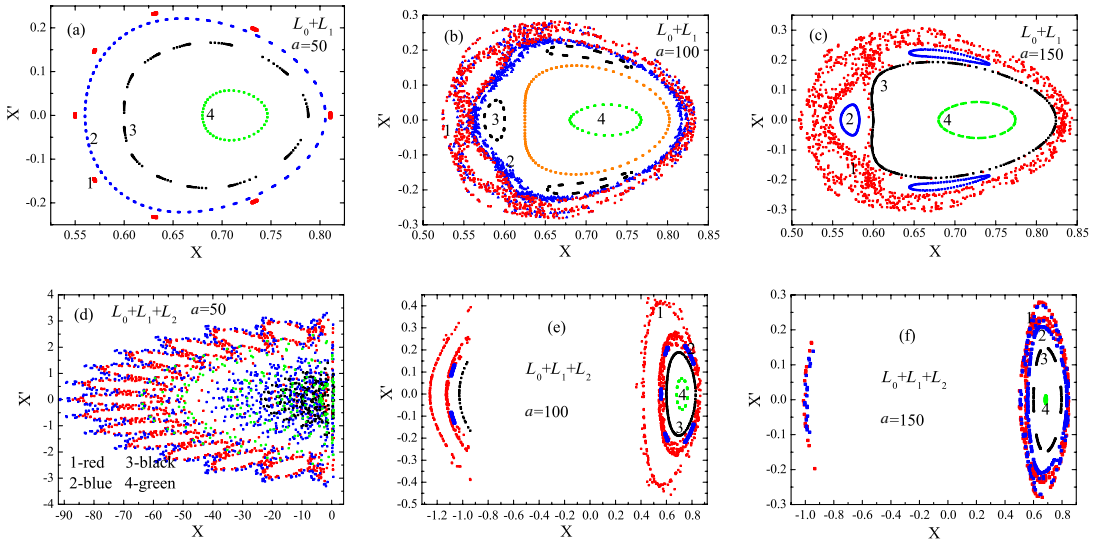

FIG. 2 (color online). Poincaré surfaces of section for the four trajectories in Fig. 1 when the PN contributions are included. Three distinct separations $a = 50$, 100, and 150 between the primary bodies are considered.

plotted clearly. Let us focus on the dynamical evolution of the four orbits when the PN effects are included.

A. The $L_0 + L_1$ system

When the PN term L_1 is added to the Newtonian part L_0, the obtained system $L_0 + L_1$ is dependent upon the separation a of the primaries. It can be seen from Fig. 2(a) that no chaos exists for $a = 50$. Here are some details of the orbital dynamical features: orbit 1 is varied from three islands to many, but originally chaotic orbit 2 or 3 evolves into a KAM torus; orbit 4 remains a torus. When $a = 100$, orbit 1 also becomes chaotic, and the chaos is stronger for orbit 1 than for orbit 2; orbit 3 turns out to have three islands. See Fig. 2(b) for more information. For $a = 150$, the dynamics differ. Figure 2(c) shows that the strength of the chaos in orbit 1 increases further, whereas three islands occur for orbit 2, and orbit 3 becomes one torus.

It can be concluded from these numerical simulations that the PN contribution from the angular speeds of the primaries is important in the orbital dynamics of the third body. In other words, the dynamics are closely related to the separation a of the primaries if a is insufficiently large. Regular single-island orbits in the Newtonian case evolve into regular multi-island orbits in the PN approximation, and even change to have strong chaoticity. On the other hand, chaotic orbits may be varied as ordered single- or multi-island orbits. In addition, the PN effect does not destroy the orbital stability at all; namely, a bounded orbit in the Newtonian counterpart cannot run to infinity and still remain bounded in the PN case. Of course, if a is extremely large, then the relativistic effect becomes too weak to affect the dynamics. This shows that the dynamics in the relativistic case are basically the same as that in the nonrelativistic case. What about the evolution of the four orbits when the PN term L_2 is also included? We explain this in subsequent sections.

B. The L system

Now, all PN contributions, L_1 and L_2, are considered. As shown in Figs. 2(d)–2(f), the dynamical properties of these orbits in the L system are completely different from those in the $L_0 + L_1$ system for the same separation a.

Taking a small separation, such as $a = 50$, we find that these orbits seem to be chaotic. However, whether they are indeed chaotic is unclear because they are unstable and the method of Poincaré section is valid only in diagnosing the dynamics of two-dimensional bounded, conservative systems. The mechanism of instability in this case is inconsistent with that of the scattering behavior of the test particle around the dynamically unstable point L_5 [20]. In our problem, such a small separation gives rise to strong relativistic effects that make the orbits unstable when the radiation reaction is turned off; however, in Ref. [20] gravitational wave losses caused the orbital instability of the test particle. In addition, the speed of the escape of orbits for the former is much slower than that for the latter.

With increased separation—for example, $a = 100$—the escape of orbits dies out. It is easy to see from Fig. 2(e) that regular orbit 1, consisting of three islands in the Newtonian case, becomes bounded and chaotic in the PN case, but chaotic orbits 2 and 3 become bounded and ordered orbits. When the separation further increases—for instance, $a = 150$—the boundedness of orbits remains. In Fig. 2(f), both orbits 1 and 2 are chaotic, but orbit 4 is almost periodic.

C. Dependence of the dynamics on a

Besides the method of Poincaré section, the method of Lyapunov exponents that characterize the average exponential deviation of two nearby orbits is a common tool to distinguish chaos from order. For convenience, the two-particle method [24,25] (in place of the variational method) is often used to calculate the largest Lyapunov exponent,

$$\lambda = \lim_{\tau\to\infty} \frac{1}{\tau} \log \frac{d(\tau)}{d(0)}, \tag{21}$$

where $d(\tau)$ and $d(0)$ denote the distances between two nearby trajectories at times τ and 0, respectively. One had better use the initial distance $d(0) \approx 10^{-8}$ in the double precision of machine and should adopt appropriate renormalization from time to time. A *bounded* orbit is said to be chaotic for $\lambda > 0$, but regular for $\lambda = 0$. In light of this, the Lyapunov exponents in Fig. 3(a) can undoubtedly indicate the regularity of orbit 1 and the chaoticity of orbit 2 in the Newtonian problem. Unfortunately, sufficiently long integration times are necessary to get these stabilizing, reliable values of Lyapunov exponents. Thus, it is computationally extremely expensive to integrate a large number of orbits.

Instead, fast Lyapunov indicators (FLIs) are a quicker method to find chaos than the method of Lyapunov exponents. They were first proposed by Froeschlé *et al.* [26], and then developed into the two-nearby-trajectories method [25] by the following equation:

$$\mathrm{FLI(t)} = \log_{10} \frac{d(t)}{d(0)}. \tag{22}$$

The choice of $d(0) = 10^{-9}$ is good. The saturation of orbits occurs due to the chaotic boundary in the case of $d(t) = 1$. Numerical integration does not last unless renormalization is implemented. If the sequential number of renormalization is k, then the indicator is practically computed by the following equation:

$$\mathrm{FLI} = -(k+1)\log_{10} d(0) + \log_{10} d(t). \tag{23}$$

A bounded orbit is chaotic if its indicator grows with time according to an exponential law, while it is regular if it does so according to an algebraic law. Through this criterion, we can know from Fig. 3(b) that orbits 1 and 2 of Fig. 1 are ordered and chaotic, respectively. Only the integration time, $\tau = 3000$, is needed to complete this task.

Since the method of FLI is superior to that of Lyapunov exponents in efficiency, it is used to trace how the dynamics of orbits 1 and 2 depend on the separation a under the PN interactions. This operation is performed for varying distances a, running from 10 to 200 with a span of $\Delta a = 1$, and the value of FLI is obtained after the integration time is added up to $\tau = 3000$ for each separation a. During this time, 5 is regarded as a threshold value of FLI between order and chaos/instability. Any orbit whose FLI is larger than the threshold is chaotic or unstable, while all orbits whose FLIs are less than the threshold are bounded and regular.

Figure 3(c) shows the relationship between the FLI and the separation a when orbit 1 in the system $L_0 + L_1$ is chosen as a test orbit. It can be shown that the orbit is always bounded in all tested cases. There are three ordered intervals of a: [10, 82], [159, 165], and [174, 200]. The FLIs at the critical values of a involving 82, 159, 165, and 174 are 2.5, 2.7, 2.4, and 4.2, respectively. As some examples to check the orbital features, the orbit consists of five islands for $a = 82$ in Fig. 4(a), and it becomes three islands for $a = 174$ in Fig. 4(b). In practice, the three

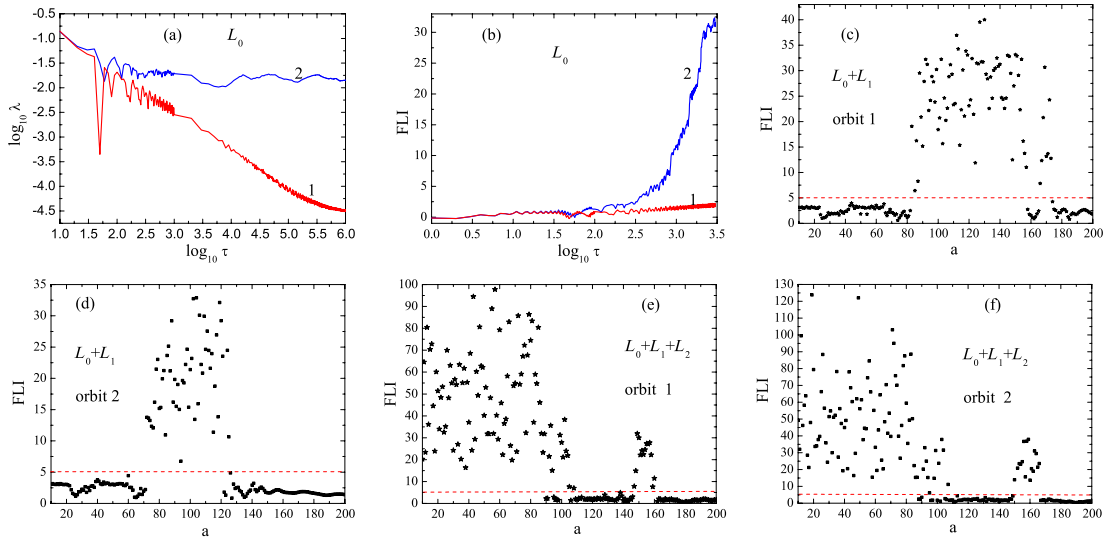

FIG. 3 (color online). (a) and (b): The Lyapunov exponents λ and FLIs of orbits 1 and 2 in Fig. 1. (c)–(f): The dependence of FLI on the separation a from 10 to 200 for orbits 1 and 2 with the PN contributions included.

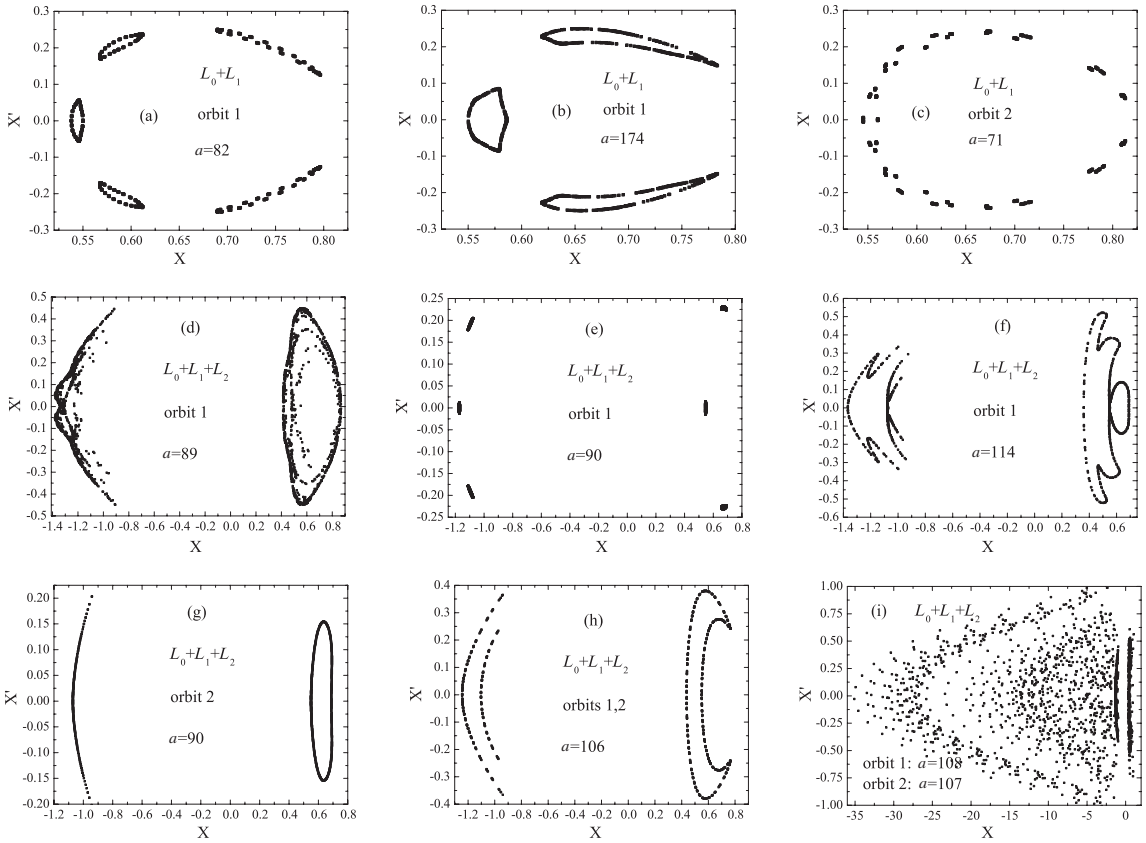

FIG. 4. Poincaré surfaces of section in certain cases of Figs. 3(c)–3(f).

islands—like those in the Newtonian counterpart—can remain when a spans 174. The remaining intervals of a, [83, 158] and [166, 173], are chaotic. The chaotic features for $a = 83$ with FLI = 19.1, $a = 157$ with FLI = 11, $a = 166$ with FLI = 7.8, and $a = 173$ with FLI = 12.7 are similar to those in Figs. 2(b) and 2(c). On the other hand, when orbit 1 is replaced by orbit 2, the dynamical evolution as a function of a is displayed in Fig. 3(d). The dynamics are ordered for $a \in [10, 71] \cup [126, 200]$, $a = 122$ or $a = 123$, while they are chaotic when $a \in [72, 121]$, $a = 124$ or $a = 125$. The critical values of a are 71, 72, 121, 122, 123, 124, 125, and 126, which correspond to FLI values of 2.2, 13.8, 23.5, 1.8, 1.3, 24.5, 10.7, and 4.8, respectively. For $a = 71$, orbit 2 is made of many islands, which are shown in Fig. 4(c). However, the orbit for $a = 72$ resembles chaotic orbit 2 in Fig. 2(b). In the case of $a = 126$, the dynamics are similar to orbit 2 with three islands in Fig. 2(c).

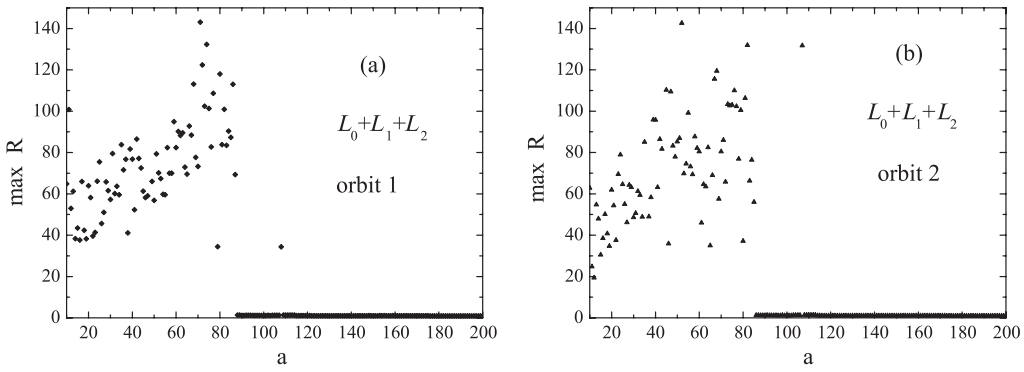

FIG. 5. Maximum values of $R = \sqrt{X^2 + Y^2}$ when the integration time is 10000 for each separation a. The maximum values of R larger than 20 will dramatically increase while the computations last, whereas those less than 1.5 are almost invariant. This implies that the former dynamics are unbounded and unstable, whereas the latter dynamics are bounded and stable. It is clear that the dynamics of orbit 1 becomes unstable for $a \in [10, 88]$ or $a = 108$, and that of orbit 2 becomes unstable for $a \in [10, 86]$ or $a = 107$.

TABLE I. Values of the separation $a \in [10, 200]$ for the dynamically unstable, bounded chaotic, and bounded regular dynamics.

Approximation	Orbit	Unstable	Order	Chaos
$L_0 + L_1$	1		[10,82], [159,165], [174,200]	[83,158], [166,173]
$L_0 + L_1$	2		[10,71], [126,200], 122, 123	[72,121], 124, 125
$L_0 + L_1 + L_2$	1	[10,88], 108	[109,146], [62,200], 90, 91	[99,105], [147,161]
			92, 95, 96, 97, 98, 106, 107	89, 93, 94
$L_0 + L_1 + L_2$	2	[10,86], 107	[108,149], [167,200], 88, 89	[91,95], [150,166], 87
			90, 96, 97, 100, 102, 105, 106	98, 99, 101, 103, 104

The dynamics of orbit 1 depending on a when the PN term L_2 is also included are shown in Fig. 3(e). The regions of separation for the FLIs beyond 5 are $a \in [10, 89] \cup [99, 105] \cup [147, 161] \cup \{93, 94, 108\}$. Maximum values of R beyond 20 during the integration time $\tau = 10000$ in Fig. 5(a) show that the values of a for the unbounded, unstable dynamics of orbit 1 are 108 and $[10, 88]$. As an example, the orbit for $a = 108$ with FLI $= 6.9$ is an unstable orbit, which is shown in Fig. 4(i) [resembling that in Fig. 2(d)]. As mentioned above, the occurrence of chaos is unclear because an unstable, unbounded orbit does not necessarily mean chaos even if an orbit and its nearby orbit diverge exponentially. In addition, in the method of FLIs—as in the methods of Lyapunov exponents and Poincaré section—it is very difficult to distinguish the exponential deviation of a chaotic orbit from that of an unstable orbit. This being the case, these chaos indicators are mainly used to diagnose the dynamics of bounded systems. Of course, bounded chaos exists for $a \in [99, 105] \cup [147, 161] \cup \{89, 93, 94\}$; see Fig. 4(d) or orbit 1 of Figs. 2(e) and 2(f) for reference. For the rest of the values in the interval [10, 200], i.e., $a \in [109, 146] \cup [62, 200] \cup \{90, 91, 92, 95, 96, 97, 98, 106, 107\}$, the dynamics are regular. The orbits in Figs. 4(e), 4(f), and 4(h) are some examples of the regular dynamics. When we use orbit 2 rather than orbit 1 as a test orbit, the dependence of the dynamics on a in Fig. 3(f) seems to be slightly different from that in Fig. 3(e). The unstable domains of a are $[10, 86] \cup \{107\}$, which are shown in Fig. 5(b). In addition, $[91, 95] \cup [150, 166] \cup \{87, 98, 99, 101, 103, 104\}$ and $[108, 149] \cup [167, 200] \cup \{88, 89, 90, 96, 97, 100, 102, 105, 106\}$ are bounded chaotic and bounded ordered domains of a, respectively. For instance, the dynamics in Figs. 4(g) and 4(h) are regular, whereas those in Fig. 4(i) are unstable.

For the reader's convenience, Table 1 lists the values of the separation a for the dynamically unstable, bounded chaotic, and bounded regular dynamics in Figs. 3(c)–3(f) and Fig. 5.

IV. SUMMARY

By means of applying scaling transformations to distance, time, velocity, and acceleration, we worked out the dynamical equations of the PN circular restricted three-body problem, derived from the PN Lagrangian. The two PN contributions, including the relativistic effects from the circular orbital frequencies between the primaries and those from the primaries to the third body, are explicitly dependent on the separation a of the parent binary. This is helpful for studying how the separation affects the dynamics of order and chaos in the PN system.

When the PN contribution from the angular speeds of the primaries is included in the Newtonian problem, the PN dynamics display a qualitatively different behavior compared with the Newtonian dynamics if the separation a of the primaries is insufficiently large. Regular single-island orbits in the Newtonian case may evolve as regular multi-island or strong chaotic orbits in the PN approximation; however, chaotic orbits may vary as ordered single- or multi-island orbits. In particular, the boundedness of orbits in the nonrelativistic case can still be maintained in the relativistic case. On the contrary, the boundedness can be destroyed when the PN contribution from the primaries to the third body is also included and the separation a is small. By investigating the dependence of the dynamics on the separation a with the FLIs, we classified the separation a into three domains for the dynamically unstable, bounded chaotic, and bounded regular dynamics. Of course, the dynamics with all PN contributions included are almost the same as that in the classic case if a is extremely large.

ACKNOWLEDGMENTS

The authors are very grateful to an anonymous referee for many good suggestions. This research is supported by the Natural Science Foundation of China under Grant Nos. 11173012 and 11178002.

[1] T. I. Maindl and R. Dvorak, Astron. Astrophys. **290**, 335 (1994).
[2] L. F. Wanex, PhD thesis, University of Nevada, Reno, 2002.
[3] F. Varadi, B. Runnegar, and M. Ghil, Astrophys. J. **592**, 620 (2003).
[4] F. Benitez and T. Gallardo, Celest. Mech. Dyn. Astron. **101**, 289 (2008).
[5] X. Wu and H. Zhang, Astrophys. J. **652**, 1466 (2006).
[6] O. Semerák and P. Suková, Mon. Not. R. Astron. Soc. **425**, 2455 (2012).
[7] P. Suková and O. Semerák, Mon. Not. R. Astron. Soc. **436**, 978 (2013).
[8] Y. Wang, X. Wu, and W. Sun, Commun. Theor. Phys. **60**, 433 (2013).
[9] J. Levin, Phys. Rev. Lett. **84**, 3515 (2000).
[10] J. Levin, Phys. Rev. D **67**, 044013 (2003).
[11] X. Wu and Y. Xie, Phys. Rev. D **77**, 103012 (2008).
[12] L. Mei, M. Ju, X. Wu, and S. Liu, Mon. Not. R. Astron. Soc. **435**, 2246 (2013).
[13] N. J. Cornish and J. Levin, Phys. Rev. D **68**, 024004 (2003).
[14] Y. Z. Wang, X. Wu, and S. Y. Zhong, Acta Phys. Sin. **61**, 160401 (2012).
[15] K. Yamada and H. Asada, Phys. Rev. D **82**, 104019 (2010).
[16] K. Yamada and H. Asada, Phys. Rev. D **86**, 124029 (2012).
[17] Z. E. Wardell, Mon. Not. R. Astron. Soc. **334**, 149 (2002).
[18] Z. E. Wardell, Mon. Not. R. Astron. Soc. **341**, 423 (2003).
[19] J. D. Schnittman, Astrophys. J. **724**, 39 (2010).
[20] M. Seto1 and T. Muto, Phys. Rev. D **81**, 103004 (2010).
[21] L. D. Landau and E. M. Lifshitz, *The classical theory of fields* (Pergamon Press, London, 1962).
[22] C. D. Murray and S. F. Dermott, *Solar System Dynamics* (Cambridge University Press, Cambridge, England, 1999).
[23] C. M. Will, Phys. Rev. D **89**, 044043 (2014).
[24] X. Wu and T. Y. Huang, Phys. Lett. A **313**, 77 (2003).
[25] X. Wu, T. Y. Huang, and H. Zhang, Phys. Rev. D **74**, 083001 (2006).
[26] C. Froeschlé, E. Lega, and R. Gonczi, Celest. Mech. Dyn. Astron. **67**, 41 (1997).